Sewage Sludge Ash: A Comparative Evaluation with Fly Ash for Potential Use as Lime-pozzolan Binders

Yi-fan Zhou[1], Jiang-shan Li[1,2,] Jian-xin Lu[1], Chris Cheeseman[3], Chi Sun Poon[1*]

1 Department of Civil and Environmental Engineering, The Hong Kong Polytechnic University, Hung Hom, Kowloon, Hong Kong

2 State Key Laboratory of Geomechanics and Geotechnical Engineering, Institute of Rock and Soil Mechanics, Chinese Academy of Sciences, Wuhan 430071, China

3 Department of Civil and Environmental Engineering, Centre for Environmental Control and Waste Management, Imperial College, London, SW7 2BU, UK

*Email: cecspoon@polyu.edu.hk

Fax: +852 2334 6389

Abstract

The disposal of sewage sludge ash (SSA) has become an environmental issue due to the limited available landfilling space. This study aims at applying the finely-ground sewage sludge ash (FSSA) with quicklime and hydrated lime respectively to develop a new type of lime-pozzolan system and study the effects of different types of lime on the mechanical properties of the systems. A traditional pozzolanic material (i.e. coal fly ash (FA)) was also used to compare with the FSSA. Multiple techniques including X-ray diffraction (XRD), scanning electron microscopy (SEM) and thermogravimetric analysis (TGA) were used to assess the hydration kinetics and microscopic characteristics of the lime-pozzolan systems.

The results showed that the quicklime system exhibited lower strength than the hydrated lime system, which was due to its lower reaction degree with the FSSA and the higher porosity caused by the expansion during the vigorous hydration reaction of quicklime.

Compared to FA, the FSSA attained higher strength for the whole curing period (up to 90 d) in the lime system due to the highly porous nature of FSSA leading to a lower effective water to binder ratio. However, in the hydrated lime system, due to the higher overall pozzolanic activity of FA, its long-term strength values gradually improved.

Besides, calcium phosphate hydrate crystals were detected by XRD in the FSSA; while some clinotobermorite was found in the FA both from XRD and SEM, which might govern the strength gain in the lime-FA system. Overall, the application of FSSA as a pozzolan in the lime-pozzolan system could be a promising option to both relieve the waste disposal pressure and provide a potential sustainable construction material.

Keywords

Finely-ground sewage sludge ash (FSSA); fly ash (FA); lime-pozzolan; hydration; construction material; waste management.

1. Introduction

Lime-pozzolan binders have been widely studied and applied in construction since ancient times. Specifically, the lime-volcanic ash mortars were first applied as a wall covering in Santorini Island in 1500 BC [1]. The Romans utilized lime together with volcanic ash and crushed sintered clay products in concrete for the construction of buildings and coastal works, which had resisted erosion from seawater for over 20 centuries [2].

However, the invention of Portland cement (PC) in the 19th century caused the recession of the use of the lime-pozzolan binders. But they have again become popular as alternatives to PC recently due to the high cost, carbon footprint and energy intensity of PC. In addition, concrete based on PC would normally suffer from long-term degradation problems, especially under harsh conditions [2]. More importantly, the application of PC-based materials on repairing ancient buildings is not allowed according to the requirements regulated by European supervisory authorities which specify that the repairing materials should be compatible with the original materials [3].

Pozzolans are commonly used as partial replacements for PC, as they are not only cost-effective, but also improve some properties of the produced mortars and concrete. The role of pozzolans in the lime-pozzolan binders is their participation in pozzolanic reactions with calcium hydroxide to form hydration products, which are similar to those produced from PC hydration including calcium silicate hydrates (CSH) and calcium aluminate silicate hydrates (CASH) [4].

Extensive studies have investigated the characteristics, hydration, carbonation and applications of lime-pozzolan pastes/mortars. They mostly focused on natural pozzolans such as volcanic ash, artificial pozzolans such as brick dust and some common industrial waste pozzolans such as fly ash (FA) and ground granulated blast furnace slag (GGBS) or a combination of these [5]. In addition, various combinations of limestone, metakaolin, natural zeolites, silica sand, crushed bricks/rocks, and siliceous wastes had been studied for the production of lime-pozzolan binders [6-8]. It was found that different pozzolans have varying pozzolanic activities [9].

Incinerated sewage sludge ash (ISSA), a by-product generated from the incineration process of sewage sludge of wastewater treatment plants, is increasingly being generated and the common management method is landfilling. Considering the limited availability of landfilling space, it is no longer a sustainable waste management solution for ISSA [10, 11]. In order to resolve this issue, different recycling methods have been developed. The characteristics of ISSA may vary significantly from place to place, but typical elemental compositions of ISSA include P, Ca, Si, Al and Fe [12]. ISSA normally only possesses a relatively low pozzolanic reactivity due to the presence of a large amount of crystallised SiO_2 and the particles are with irregular shapes and large porosity [13, 14]. Even so, as a valuable

resource, the ISSA has a great potential to be applied for the production of cement, aggregates, mortars, concrete and controlled low-strength materials [15]. In addition, many researchers have studied the use of ISSA as supplementary cementitious materials [11, 16-18] and for soil stabilisation [19-21].

For its application in the cement-based materials as a pozzolan, it was found that 20% replacement of cement with ISSA would not adversely affect the mortar strength [11]. The pozzolanic activity of ISSA was found to be lower than FA, but the ISSA could still improve the strength of mortars containing ISSA at the later curing stage [22]. At 5% and 10% replacement levels, the 28-day mortar strengths were comparable to the control [23]. Increase the fineness of ISSA by grinding could improve the mechanical properties through enhancement of its pozzolanic activity [24]. Generally, the ISSA could be used as a low-grade pozzolan which can save natural resources for cement production and the associated carbon emissions [10, 17].

The use of wastes as secondary building materials has attracted increasing attention due to environmental protection issues. Using the ISSA as a binder for soil stabilisation has been demonstrated to help to facilitate the use of soft soils [25]. Some studies used up to 16% ISSA to treat cohesive soils or clay and obtained improved geotechnical properties such as increased unconfined compressive strength and decreased swelling pressure [19, 26]. However, in order to have higher strength, a small portion of cement or hydrated lime were added to promote the pozzolanic reaction of ISSA [27-29]. A previous study reported that a maximum of 26% strength increase was attained in the soil-cement mixture with 20% ISSA [20]. By using ISSA and hydrated lime, soft subgrade soil could be stabilised to achieve 3 to 7 times higher unconfined compressive strength and improved shear strength. It was also concluded that an 8% ISSA-hydrated lime mixture was the optimal content added in the soils for effective stabilisation treatment [28].

Different types of lime also affected the reactions with the pozzolans and hence the strength development. The heat liberated from quicklime (CaO) hydration could accelerate the early pozzolanic reactions, because the freshly-produced $Ca(OH)_2$ from lime hydration had a higher solubility than the commercially-available hydrated lime ($Ca(OH)_2$) [30]. It was found that the hydrated lime-pozzolan pastes had a higher porosity than the lime-pozzolan pastes, which dedicated that higher compressive strength was obtained by the lime-pozzolan pastes [30].

However, very limited information is available on the lime- sewage sludge ash (SSA) system. In order to better understand the reactions between quicklime/hydrated lime and SSA, finely-ground SSA (FSSA) that possessed a relatively higher pozzolanic activity than the as-received SSA was used in this study. FA, as a representative of common supplementary cementitious materials, was also used for comparison. The hydration heat of the fresh pastes and the mechanical properties of the hardened pastes were evaluated. The reaction products and

microstructural properties were assessed by using X-ray diffraction (XRD), scanning-electron microscopy (SEM) and thermogravimetric analysis (TGA) to elucidate the mechanisms governing its performance.

2. Materials and methods

2.1 Materials

The FSSA used in this study was collected from the T-Park (a sewage sludge incineration plant) in Hong Kong. The ash was dried in a 105°C oven overnight and finely ground in a ball mill for two hours. The quicklime and hydrated lime were commercially available from local suppliers, and FA was provided by a local coal power plant.

The particle size distributions of quicklime (lime, CaO), hydrated lime (CH), FSSA and FA measured by using a Malvern Mastersizer 3000 are presented in Fig. 1. The mean particle sizes were 27.48, 40.11, 23.77 and 26.6 μm for lime, hydrated lime, FSSA and FA, respectively. The FSSA particles were slightly finer than the FA particles.

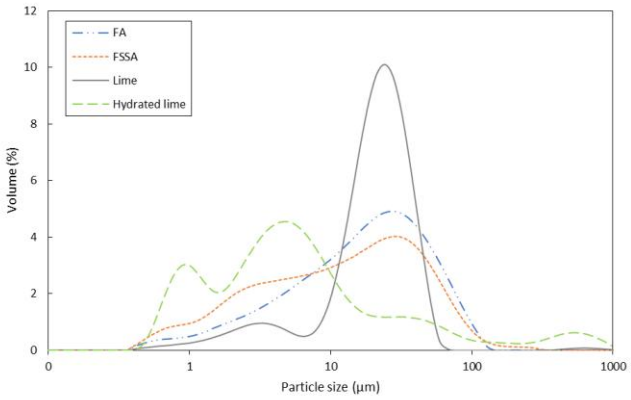

Fig. 1 Particle size distributions of raw materials

The morphologies of gold-coated FSSA and FA samples were obtained by using a scanning electron microscope (SEM, TESCAN VEGA3), as presented in Fig. 2. It is clear that the FSSA particles were porous and a relatively rough surface. The FA particles were largely spherical in shape. Fig. 3 presents the XRD spectra of FSSA and FA. The main crystalline phases of FSSA are quartz (SiO_2), hematite (Fe_2O_3), magnetite (Fe_3O_4), leucite ($KAlSi_2O_6$) and anorthoclase ((Na,K)AlSi3O8). In the FA, there are mainly quartz, mullite ($3Al_2O_3{\cdot}2SiO_2$), magnetite, and hematite.

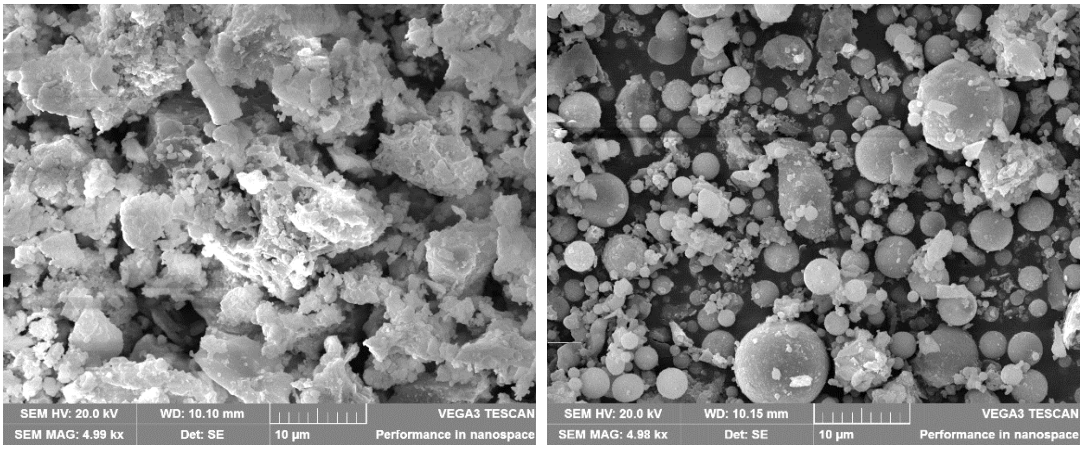

(a) FSSA (b) FA

Fig. 2 SEM images of (a) FSSA and (b) FA

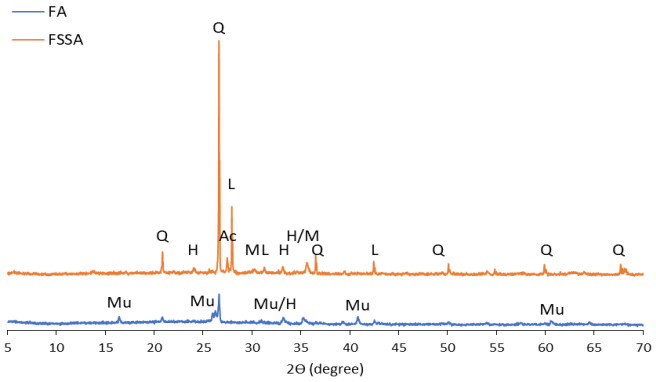

Fig. 3 XRD patterns of FSSA and FA (Q: quartz; Mu: mullite; L: leucite; H: hematite; M: magnetite; Ac: anorthoclase)

The chemical compositions of quicklime, hydrated lime, FSSA and FA determined by using a Rigaku Supermini200 X-ray fluorescence (XRF), are shown in Table 1. The major constituents of FSSA were SiO_2, Al_2O_3 and Fe_2O_3 and the FA was mainly consisted of SiO_2 and Al_2O_3. The Brunauer-Emmett-Teller (BET, Micromeritics ASAP 2020 PLUS) surface areas and loss on ignition (LOI) of raw materials under 950°C are also listed in Table 1.

Table 1. Oxide compositions (%) and physical characteristics of materials

Oxides	Hydrated lime	Quicklime	FSSA	FA
SiO_2	1.22	1.47	37.04	44.42
Al_2O_3	0.15	0.68	15.24	32.56
Fe_2O_3	0.13	0.16	14.03	6.49
CaO	97.69	96.56	6.91	6.67
MgO	0.59	0.72	2.80	1.86
K_2O	0.06	0.12	2.77	1.81
Na_2O	/	/	7.11	1.79
TiO_2	/	/	0.38	1.24
SO_3	/	0.13	3.66	2.27
P_2O_5	0.12	0.12	9.12	0.44
BET (m^2/kg)	10889	3479	2866	1742
Specific gravity (kg/m^3)	2210	3340	2740	2330
LOI (%)	/	/	1.41	3.76

2.2 Paste samples preparation

The pastes preparation followed the mix design in Table 2 and the water to binder (w/b) ratio was fixed at 0.38 for all the mixes, as several w/b ratios were tried and 0.38 was able to produce a cohesive mixture without bleeding.

Table 2. Mix design of different mixtures

Sample ID	Quicklime	Hydrated lime	FSSA/ FA	w/b	Curing age
Control			1	0.38	
10%lime-FSSA/FA	0.1		0.9	0.38	
20%lime-FSSA/FA	0.2		0.8	0.38	
30%lime-FSSA/FA	0.3		0.7	0.38	7, 28 &
10%CH-FSSA/FA		0.1	0.9	0.38	90d
20%CH-FSSA/FA		0.2	0.8	0.38	
30%CH-FSSA/FA		0.3	0.7	0.38	

The powder was dry mixed for one minute at a low speed by a standard mechanical drum mixer before adding water, and then another three minutes of mixing (1 min at low speed, 2 mins at high speed) was carried out to obtain the homogenous pastes. After mixing, the fresh mixture was cast into cubic steel moulds with a size of 20*20*20 mm and then subjected to vibration for about one minute to remove entrapped air in the samples. Lastly, the moulds were covered by a plastic film and placed at room temperature (about 25 °C) for three days. Afterwards, the pastes were demoulded and subsequently placed in an environmental chamber controlled at 95% RH and 23±2 °C until testing.

2.3 Testing programme

2.3.1 Thermal liberation of fresh pastes

A Calmetrix I-Cal 4000 calorimeter was used to perform the isothermal calorimetry test where 10~30 wt.% lime and hydrated lime was used to replace FSSA and FA. The fresh pastes first were mixed outside the calorimeter at 500 rpm for three minutes and then placed

in the four-channel calorimeter which recorded the heat evolution profiles at 20°C for 72 hours.

2.3.2 Compressive strength of harden pastes

For the compressive strength test, the 20*20*20 mm cubic paste samples were tested by a TESTOMETRIC CXM loading machine. The loading rate was 0.3mm/min and triplicates were tested to obtain the average strength values.

2.3.3 Microscopic and chemical analysis

Small pieces of the broken paste samples were placed in absolute ethanol (99.8%+, International Laboratory USA) for one week to arrest the hydration. After solvent exchange, the samples were kept in a vacuum desiccator for three days prior to the tests. For TGA and XRD tests, further grinding manually in an agate mortar and sieving (< 75 μm) was necessary. The crystalline-phase mineralogy of the samples was evaluated by using a high-resolution powdered X-ray diffractometer (Rigaku SmartLab, Japan) under the condition of 20 mA and 40 kV with CuKα radiation. The 2θ range of 5 to 70° with a step interval of 5°/min was used in the tests. Then, a Highscore plus software with an ICDD PDF 2010 database (International Centre for Diffraction Data, Powder Diffraction File) was used to identify the peaks.

For the SEM test, the representative fresh fractured surfaces of the pastes were selected, and gold coated first. Their morphologies and element distributions were then tested by using a SEM-energy dispersive X-ray (EDX) analyser operating at a working tension of 20 kV.

A Rigaku Thermo Plus EVO2 was used for TGA. A total of 10 mg sample was heated from 50 to 1000°C with a rate of 10°C/min, under 20 ml/min Argon flux. The weight loss from TGA at different temperature ranges was useful for quantifying the content of $Ca(OH)_2$ and $CaCO_3$.

3. Results and discussion

3.1 Hydration evolution

Fig. 4 shows the cumulative hydration heat of hydration of both the quicklime (lime) and hydrated-lime (CH) pastes preapred with FSSA and FA incorporation. From Fig. 4 (a), it is clear that the total heat evoloved increased with a greater amount of lime with both the FSSA and FA pastes, and the total heat of the lime-FSSA pastes was larger than that of the lime-FA pastes at all replacement levels within the first 72 hours. This may indicate that higher reaction rate and degree were achieved by FSSA due to its larger surface area and lower effective w/b ratio as the porous FSSA particles took up a certain quanity of the mixing water. The evlolved heat of the quicklime pastes mainly came from the lime dissolution and the generated heat probably promoted the reactions between lime and FSSA/FA. This is consistent with the gradually increased gradients of the heat flow curves when higher amounts

of lime were employed. Therefore, the use of lime indeed accelerated the lime-FSSA/FA reactions at the early stage, especially within the first 24 hours.

However, as shown in Fig. 4 (b), the cumulative heat evolution of the CH pastes was very low compared with the quicklime pastes and could be nearly regarded as neglectable, even though a higher amount of CH led to greater amounts of heat. This may be because the CH was relatively insoluble in water and could not react with the FSSA/FA immediately at the early age. As mentioned by Shi [30], several days were needed to reach the dissolution equilibrium of $Ca(OH)_2$. The extremely low amount of heat evolved rendered the calorimeter very susceptible and sensentive to the changes in the room temperature at which the calorimeter was placed. That might explain why there were fluctuations of the measured values. The total heat generation of the CH-FSSA pastes was also greater than that of the CH-FA pastes at all replacement levels, which again verified the higher reaction rate and degree of FSSA compared with FA within 72 hours.

For better interpretation of the differences between the lime and CH system, the heat evolution rate of the lime-FSSA paste was plotted to compare with that of the CH-FSSA paste, as presented in Fig. 4 (b). There was a sharp peak at around 10 hours after mixing which corresponded to the lime-FSSA reactions and the higher peak rate was attained by a higher amount of lime. The sharpness could be due to the very fine particles of FSSA and its large surface area. However, in the CH system, the scale of heat evolution rate (Y-axis) was much smaller than the lime system and the seemingly regular fluctuations can be attributed to the sensitivity of the calorimeter to daily temperature changes of the laboratory environment.

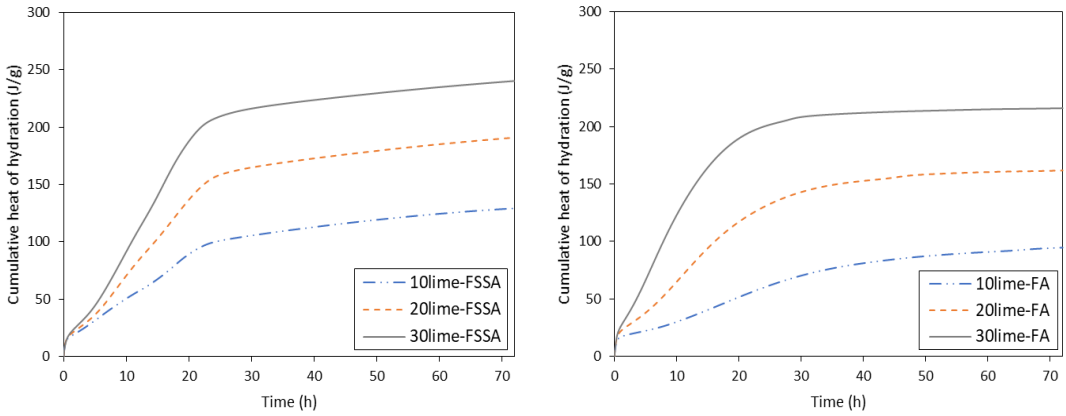

(a)

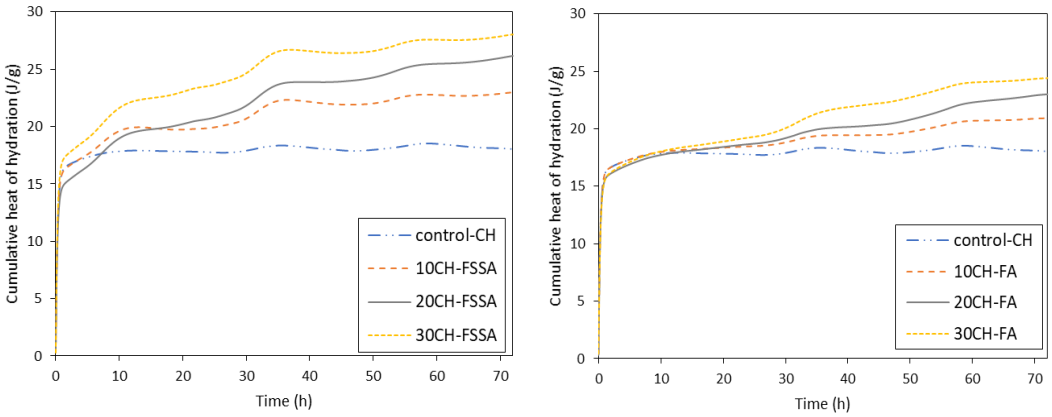

(b)

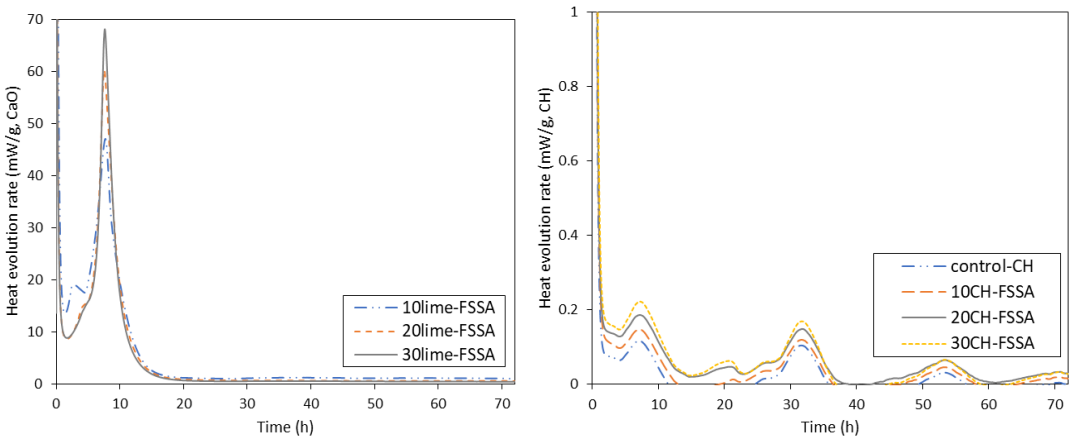

(c)

Fig. 4. Heat flows of (a) lime-FSSA/FA, (b) CH-FSSA/FA pastes, and (c) Heat evolution rates of lime-FSSA & CH-FSSA

3.2 Compressive strength

The compressive strength of the lime/CH pastes containing FSSA and FA at the curing age of 7, 28 and 90 days are presented in Fig. 5. As shown in Fig. 5 (a), a higher compressive strength was obtained by the lime-FSSA pastes than the lime-FA pastes at all curing ages. This was also consistent with the higher cumulative hydration heat of the lime-FSSA pastes in the previous section. Donatello and Cheeseman [12] concluded that SSA had a strongly positive pozzolanic activity in the saturated lime test. The strength of the lime-FSSA pastes increased with the increasing amount of lime used (from 10% to 30%) at all the studied curing time. However, the lime-FA pastes showed much lower strength than the lime-FSSA pastes at 7 and 28 days, while the strength suddenly picked up at 90 days as the FA was mostly activated and reacted at the later age [31]. The higher strength of the lime-FSSA paste at the early age was partly attributed to the lower effective w/b ratio due to the high water adsorptivity of porous FSSA particles [22]. Besides, it had been suggested that the reaction between $Ca(OH)_2$ and SSA had mechanical outcomes as they led to moderate but critical

strengthening of the pastes at 21 and 150 days [18]. Therefore, it can be envisaged that some new phases formed in the lime-FSSA pastes contributed to the strength development.

It can be seen that from Fig. 5 (b) the 20% and 30% CH-FSSA pastes had similar strength values and were much higher strength than the 10% CH-FSSA pastes. One possible reason was that 10% of CH was too little to well react with the FSSA. The strength of the CH-FSSA pastes almost linearly increased with the curing time. For the CH-FA pastes, all the strength values were comparable at 7 days, and were lower than that of the CH-FSSA pastes, which might be due to the slow pozzolanic reaction of FA at the early stage. Also, there might be insufficient soluble $Ca(OH)_2$ for the reaction with FA. Helmuth [32] found that the minimum amount of $Ca(OH)_2$ for complete reaction with class F FA was 45% by weight. However, after 28 days of curing, the CH-FA pastes experienced a faster rate of strength gain and the strength increased with the higher amount of CH. When the curing age was extended to 90 days, the strength values attained were even higher than the strengths of the CH-FSSA pastes at each level of CH addition. That was because the FA had a higher overall pozzolanic reactivity than the FSSA, which was confirmed by using the R3 method [Ali submitted manuscript to CBM]. This was related to more amorphous (reactive) phases were present in FA than FSSA providing more precursors for the formation of hydration products [22, 32].

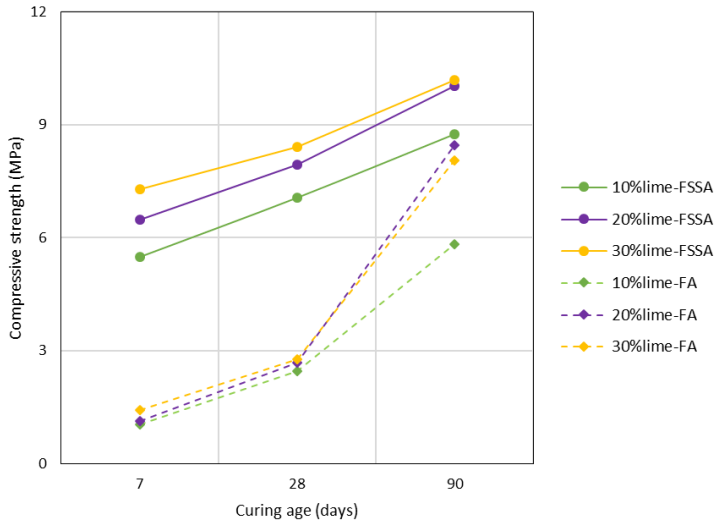

(a)

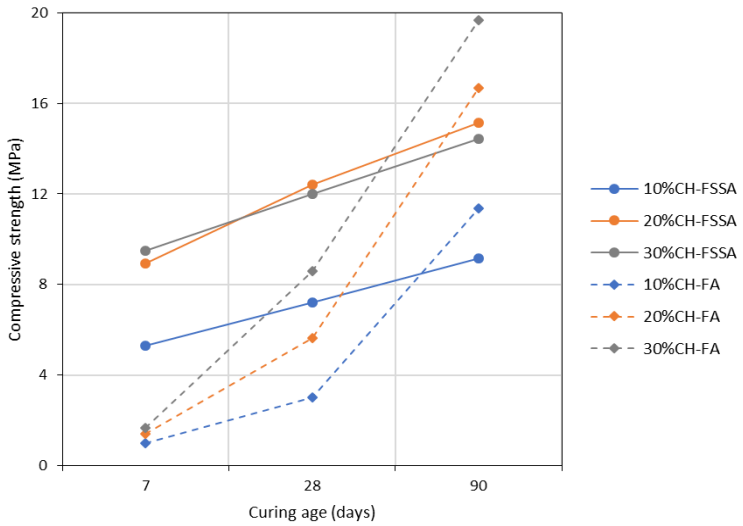

(b)

Fig. 5. Compressive strength of (a) lime pastes and (b) CH pastes with FSSA and FA

Apart from that, the slight expansions of the lime system due to exothermic reactions of lime hydration were observed which might cause some micro cracks in the paste matrix reducing the strength of the lime system. The strength difference within each system was also dependent on the consumption/reaction degree of $Ca(OH)_2$ which will be discussed in section 2.4.

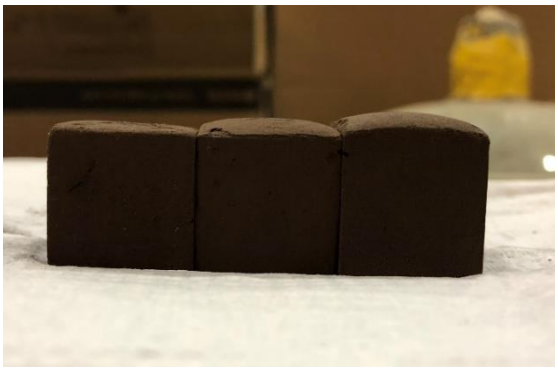

Fig. 6. Photo of lime-FSSA pastes showing slight expansion (10%~30% quicklime from left to right)

3.3 Microstructural analyses

3.3.1 Crystalline phases by XRD analyses

The XRD spectra of lime and CH pastes prepared with FSSA and FA at 28 and 90 days are presented in Fig. 7. As depicted in Fig. 7 (a), anorthoclase (Ac), hematite (H) and leucite (L) were the original phases of FSSA. Calcium phosphate hydrates (CPH) were newly formed in the lime-FSSA pastes. According to Donatello and Cheeseman [12], phosphorous (P) existed as $Ca_3(PO_4)_2$ in the SSA. Hence, the formation of CPH could be deduced as the following reaction:

$$Ca_3(PO_4)_2 + CaO + 6H_2O \rightarrow Ca_2(P_2O_7)\cdot(H_2O)_4 + 2Ca(OH)_2$$

A new phase (brushite) was also weakly detected in the lime-FSSA pastes, especially at 90 days. Besides, the calcite peaks were barely present at 28 days but became distinguishable at 90 days due to the continuing carbonation of lime.

For the lime-FA pastes (Fig. 7 (a)), except the phases that were originally present in the FA (mullite, quartz, hematite/magnetite), calcite and portlandite peaks were detected at both 28 and 90 days, especially for the intensive peaks of portlandite. This might indicate the moderate reactions between FA and lime, resulting in the lower strength of the lime-FA pastes, compared with the lime-FSSA pastes. Besides, at both curing ages, the formation of calcium silicates – (clinotobermorite) was also observed due to the pozzolanic reactions between $Ca(OH)_2$ and FA. According to He et al. [33], clinotobermorite was produced in cement pastes prepared with FA [34].

As shown in Fig. 7 (b), portlandite was weakly detected in the CH-FSSA paste, and the 90-d peak intensity slightly decreased when compared to 28-d, due to the pozzolanic reactions between $Ca(OH)_2$ and FSSA. The produced CPH was only present at 28 days, and it is noted that calcite due to its limited amount was not identified by XRD.

The CH-FA paste at 28 days showed strong intensities of clinotobermorite, suggesting its relative higher amount in the paste. However, the relative amount of clinotobermorite significantly decreased after reaching 90 days. Compared with the lime-FA pastes, the calcite peak in the CH-FA paste was much weaker, as the former porous lime pastes were easier to be carbonated.

Based on the above, the CPH and clinotobermorite might separately contribute to the strength gain of the lime-FSSA and the lime-FA pastes, while these phases could only be beneficial for the strength gain of the CH-FSSA/FA pastes at a rather late stage. However, some amorphous phases that could not be identified by XRD will be investigated in the following section.

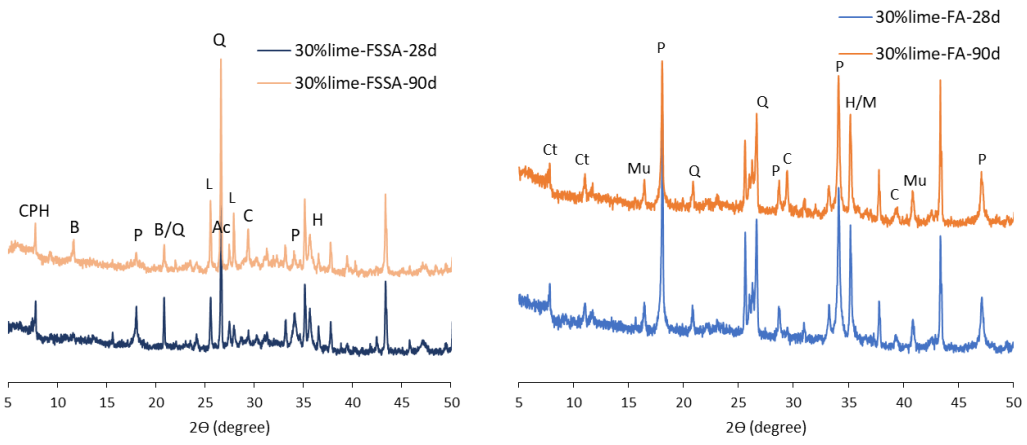

(a)

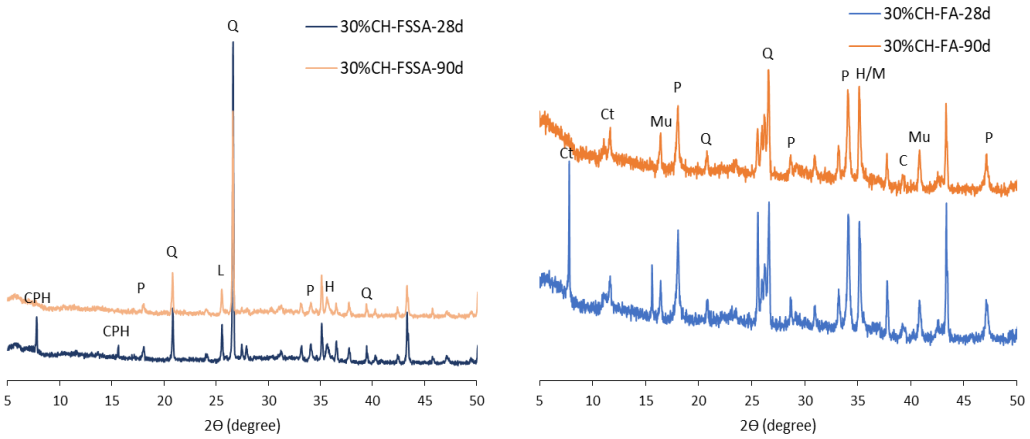

(b)

Fig. 7. XRD spectra of 30% (a) lime pastes and (b) CH pastes, at 28 & 90d (CPH: Calcium phosphate hydrate $Ca_2(P_2O_7)(H_2O)_4$; B: Brushite ($CaHPO_4 \cdot 2H_2O$); C: Calcite ($CaCO_3$); P: Portlandite; Ct: Clinotobermorite; H: Hematite; M: Magnetite; L: Leucite; Ac: Anorthoclase; Q: Quartz; Mu: Mullite)

3.3.2 SEM

Fig. 8 shows the selected SEM images together with EDX results obtained from the 30% lime and CH pastes prepared with FSSA and FA respectively after 28- and 90-day curing. In Fig. 8(a), it can be seen that the calcium alumina silicate hydrate (CASH) and CSH gels were formed and the structure of the 28-d lime-FSSA paste was less dense than that of the 90-d paste (Fig. 8 (b)). In the lime-FSSA paste at 90 days, there were some unreacted FSSA particles intersecting with CSH gels.

For the lime-FA pastes, as shown in Figs. 8 (c) and (d), significant amounts of hydration products were formed and covered the spherical FA particles, some of which were still visible, suggesting the relatively low reactivity between FA and lime. The pores in the pastes were gradually filled with those hydration products that made the microstructure of the hydrated matrix denser, leading to the strength improvement at 90 days [35]. This agreed well with the strength results of the lime-FA pastes.

In Fig. 8 (e), there were some calcite crystals located inside and on the surface of the FSSA particles. But after 90 days (Fig. 8 (f)), the FSSA particles were almost covered by hydration products and the paste structure became much denser, compared with the 28-d paste. Similar findings could be seen in the CH-FA pastes too, shown in Fig. 8 (g) and (h). calcite crystals were also present at both curing ages and some unreacted FA particles were observed in Fig. 8 (g). However, the spherical FA particles and platy portlandite crystals were hardly seen after 90 days of curing, indicating high consumption of $Ca(OH)_2$. This explained that the strength of the CH-FA pastes caught up with that of the CH-FSSA paste at this age. Besides, less pores

can be found in the 90-d paste, which was consistent with a noticeable increase in the strength development. Also, except for the crystallised clinotobermorite, some amorphous CSH could be observed in the CH-FA paste at 28 and 90 days. Based on EDX spectrum in Fig. 8 (g1), the Ca/Si ratio was about 0.82, similar to 0.83 which was the Ca/Si ratio of 11.3 Å tobermorite (clinotobermorite) [36, 37].

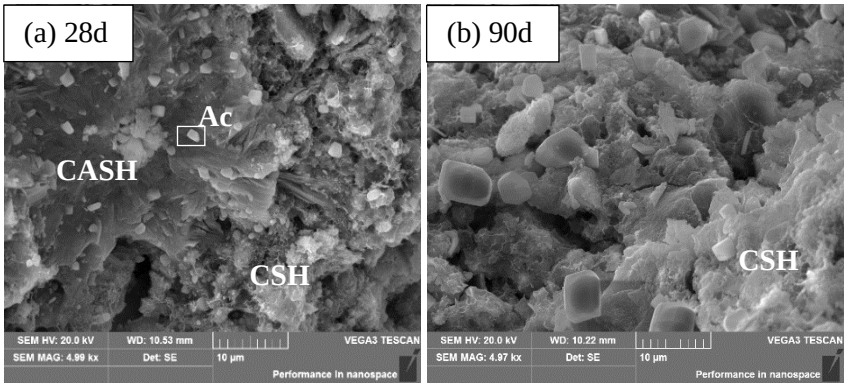

lime-FSSA

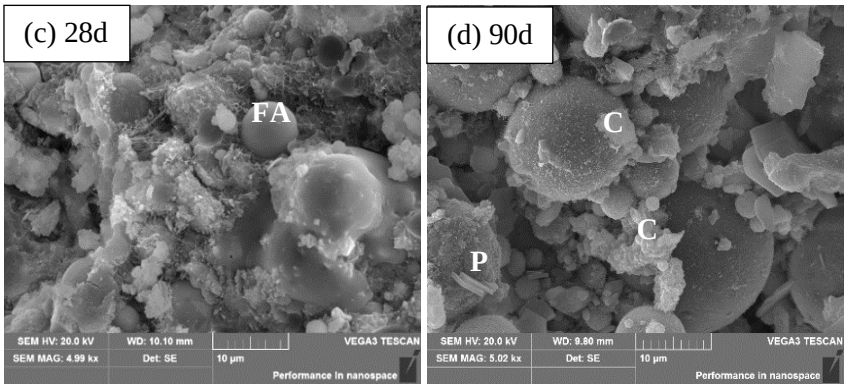

lime-FA

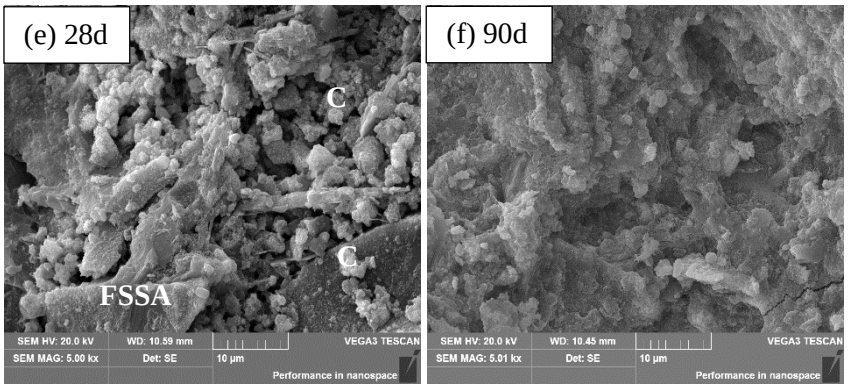

CH-FSSA

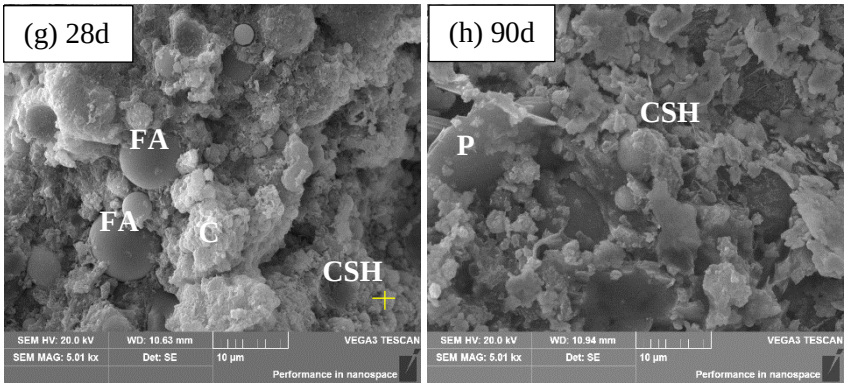

CH-FA

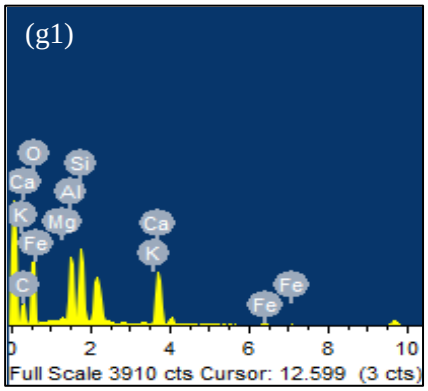

Element	Weight (%)	Atomic (%)
C K	26.79	39.58
O K	44.95	47.34
Al K	7.51	4.69
Si K	8.83	5.30
P K	0.93	0.88
K K	0.25	0.11
Ca K	10.39	4.37
Fe K	0.69	0.21
Total	100	

Fig. 8. SEM micrographs of the lime-FSSA pastes (a) 28d, (b) 90d; lime-FA pastes (c) 28d, (d) 90d; CH-FSSA pastes (e) 28d, (f) 90d; CH-FA pastes (g) 28d, (h) 90d; and (g1) EDX result of (g)

3.4 TGA results

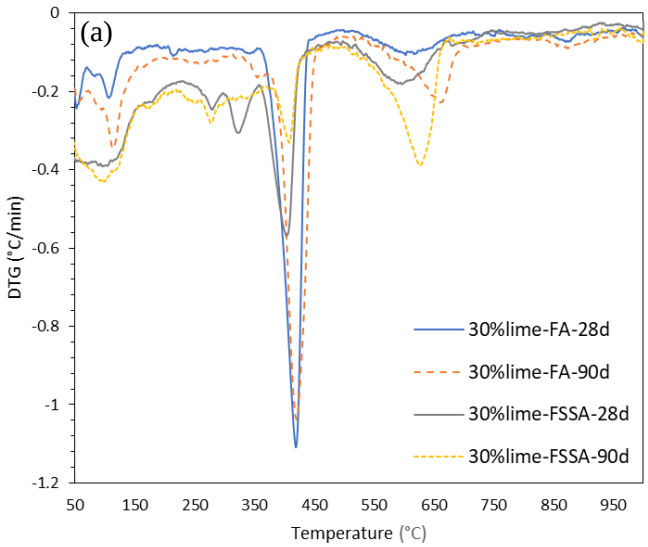

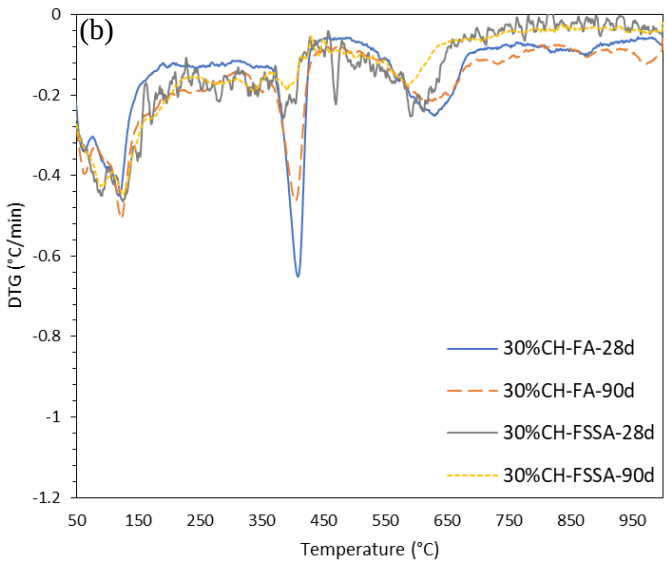

372

373 Fig. 9. DTG profiles of (a) lime pastes and (b) CH pastes at the curing age of 28 & 90 days

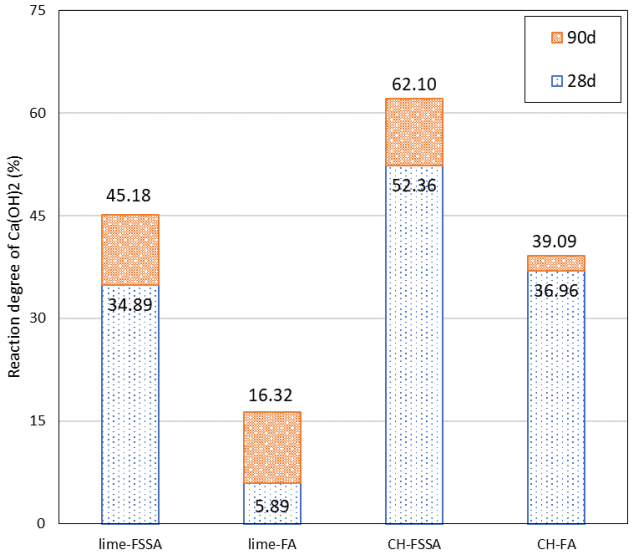

374

375 Fig. 10. Reaction degree of calcium hydroxide of lime/CH pastes containing FSSA, FA at 28
376 and 90d

377 The DTG data of 30% lime/CH pastes containing FSSA and FA at the curing ages of 28 and
378 90 days are plotted in Fig. 9. The main endothermic peak around 450°C was attributed to
379 dehydroxylation of $Ca(OH)_2$ and that at the temperature range of 600-800°C was
380 corresponded to the decarbonation of calcium carbonates (CC). For the lime system (Fig. 9
381 (a)), the lime-FA pastes had a much stronger dehydroxylation peak of $Ca(OH)_2$ than the lime-
382 FSSA pastes. Fig. 10 illustrates the reaction degree of CH in both the lime and CH pastes. The
383 reaction degree of $Ca(OH)_2$ was computed by the following equation:

$$\text{Ca}(OH)_2 \text{ reaction degree } (\%) = 100 - \text{Ca}(OH)_2 \text{ content } (\%)$$
$$= 100 - (4.11\text{MassCa}(OH)_2 + 1.68\text{MassCC})$$

where Mass$Ca(OH)_2$ is the mass loss (%) of $Ca(OH)_2$ decomposition between 350-500°C, MassCC is the mass loss (%) of CC decomposition between 550-750°C [38].

It can be seen that a significant amount of $Ca(OH)_2$ was left in the lime-FA pastes and the amount remained relatively stable with the curing time. This may explain the relatively lower reactivity and strength of the lime-FA pastes, implying that the FSSA was more reactive in the lime system than the FA. Also, a high content of unreacted $Ca(OH)_2$ was left in the lime-FA pastes lowered the strength of the lime-FA paste [30].

For the lime-FSSA pastes, the reduction of $Ca(OH)_2$ content suggested a much higher reaction degree of FSSA in the lime system, as shown in Fig. 10. It is noteworthy that another small peak was observed between 260-320°C in the lime-FSSA paste, which might be attributed to decomposition of CPH, as a previous study reported that the hydrated calcium phosphate dehydrated at around 300°C [39]. CPH was also identified in the XRD results. The decarbonation peak was mainly due to the carbonation of lime and became more obvious from 28 to 90 days.

As shown in Fig. 9 (b), at the same curing age, the $Ca(OH)_2$ decomposition peak intensity of the CH-FSSA pastes was much weaker than that of the CH-FA pastes. Also, the CH-FSSA showed a higher reaction degree of $Ca(OH)_2$ than the CH-FA pastes at 28 and 90 days (Fig. 10), which meant that the FSSA consumed more $Ca(OH)_2$ than the FA. This finding was consistent with the higher strength value of the CH-FSSA pastes at 28 days. However, even though the CH-FA paste showed a lower $Ca(OH)_2$ reaction degree at 90 days, the strength of the CH-FA paste was higher than that of the CH-FSSA paste. This may be attributed to a higher content of CC in the CH-FA paste at the later age leading to a lower reaction degree and a higher pozzolanic activity of FA.

4. Conclusion

The use of lime and hydrated lime had different influences on the pozzolanic reactions and strength development of the FSSA and FA pastes. The findings from the study may provide a potential new type of lime-pozzolan binder option by recycling sewage sludge ash. The following conclusions can be drawn from this study:

(1) The FSSA generated a higher amount of hydration heat and reacted faster than the FA in the lime pastes, while the CH pastes generated very little amount of heat with both FSSA and FA. The heat produced from lime hydration accelerated the reactions between FSSA/FA but induced expansion to the paste samples.

(2) In both quicklime and hydrated lime systems, the strength of FSSA pastes were higher than that of FA pastes at the early curing ages due to the porous nature of

FSSA which enabled a lower effective w/b ratio. The CH-FA pastes showed a comparable strength in the long term due to the higher pozzolanic activity of FA.

(3) The use of FSSA was beneficial for the management of wastes with very high water contents such as contaminated marine sediments.

Acknowledgements

The first author would like to thank The Hong Kong Government PhD Fellowship Scheme for financial support and this research was also supported by the National Natural Science Foundation of China/Hong Kong Research Grants Council Joint Research Scheme under grant No. N_PolyU511/18.

References

[1] Grist ER, Paine KA, Heath A, Norman J, Pinder H. Compressive strength development of binary and ternary lime–pozzolan mortars. Materials & Design (1980-2015). 2013;52:514-23.

[2] Witze A. Seawater is the secret to long-lasting Roman concrete. Nature news. 2017.

[3] Maravelaki-Kalaitzaki P, Bakolas A, Moropoulou A. Physico-chemical study of Cretan ancient mortars. Cement and Concrete Research. 2003;33(5):651-61.

[4] Building Conservation. Pozzolans for Lime Mortars. <http://www.buildingconservation.com/articles/pozzo/lime-pozzolans.htm>. 2010.

[5] Zhu C, Lu P. Alkali feldspar dissolution and secondary mineral precipitation in batch systems: 3. Saturation states of product minerals and reaction paths. Geochimica et Cosmochimica Acta. 2009;73(11):3171-200.

[6] Maravelaki-Kalaitzaki P, Bakolas A, Karatasios I, Kilikoglou V. Hydraulic lime mortars for the restoration of historic masonry in Crete. Cement and Concrete Research. 2005;35(8):1577-86.

[7] Černý R, Kunca A, Tydlitát V, Drchalová J, Rovnaníková P. Effect of pozzolanic admixtures on mechanical, thermal and hygric properties of lime plasters. Construction and Building Materials. 2006;20(10):849-57.

[8] Snellings R, Mertens G, Hertsens S, Elsen J. The zeolite–lime pozzolanic reaction: Reaction kinetics and products by in situ synchrotron X-ray powder diffraction. Microporous and Mesoporous Materials. 2009;126(1):40-9.

[9] Pavía S. Behaviour and Properties of Lime-Pozzolan Pastes. 2019.

[10] Dhir RK, Ghataora GS, Lynn CJ. 1 - Introduction. In: Dhir RK, Ghataora GS, Lynn CJ, editors. Sustainable Construction Materials: Woodhead Publishing; 2017. p. 1-8.

[11] Chen Z, Poon CS. Comparing the use of sewage sludge ash and glass powder in cement mortars. Environmental technology. 2016;38:1-20.
[12] Donatello S, Cheeseman CR. Recycling and recovery routes for incinerated sewage sludge ash (ISSA): A review. Waste Management. 2013;33(11):2328-40.
[13] Tantawy M, El-Roudi A, Abdalla E, Abdelzaher M. Evaluation of the Pozzolanic Activity of Sewage Sludge Ash. ISRN Chemical Engineering. 2012.
[14] Yusuf R, Zainon Noor Z, Din Md, Abba A. . Use of sewage sludge ash (SSA) in the production of cement and concrete – A review. International Journal of Global Environmental Issues. 2012;12:214-28.
[15] Dhir RK, Ghataora GS, Lynn CJ. 4 - Sewage Sludge Ash Characteristics. In: Dhir RK, Ghataora GS, Lynn CJ, editors. Sustainable Construction Materials: Woodhead Publishing; 2017. p. 69-110.
[16] Chen Z, Li JS, Poon CS. Combined use of sewage sludge ash and recycled glass cullet for the production of concrete blocks. Journal of Cleaner Production. 2018;171:1447-59.
[17] Vouk D, Nakic D, Stirmer N, Cheeseman CR. Use of sewage sludge ash in cementitious materials. Rev Adv Mater Sci. 2017;49 (2017) 158-170.
[18] Cyr M, Coutand M, Clastres P. Technological and environmental behavior of sewage sludge ash (SSA) in cement-based materials. Cement and Concrete Research. 2007;37(8):1278-89.
[19] AI-Sharif MM, Attom MF. A geoenvironmental application of burned wastewater sludge ash in soil stabilization. Environmental Earth Sciences. 2014;71(5):2453-63.
[20] Ingunza MPD, Pereira KLdA, Junior OFdS. Use of Sludge Ash as a Stabilizing Additive in Soil-Cement Mixtures for Use in Road Pavements. Journal of Materials in Civil Engineering. 2015;27(7):06014027.
[21] Lin D-F, Lin K-L, Luo H-L. A Comparison between Sludge Ash and Fly Ash on the Improvement in Soft Soil. Journal of the Air & Waste Management Association (1995). 2007;57:59-64.
[22] Chen Z, Poon CS. Comparative studies on the effects of sewage sludge ash and fly ash on cement hydration and properties of cement mortars. Construction and Building Materials. 2017;154:791-803.
[23] Naamane S, Rais Z, Taleb M, Mtarfi NH, Sfaira M. Sewage sludge ashes: Application in construction materials. 2016;7:67-72.
[24] Pan S-C, Tseng D-H, Lee C-C, Lee C. Influence of the fineness of sewage sludge ash on the mortar properties. Cement and Concrete Research. 2003;33(11):1749-54.
[25] Dhir RK, Ghataora GS, Lynn CJ. 7 - Geotechnical Applications. In: Dhir RK, Ghataora GS, Lynn CJ, editors. Sustainable Construction Materials: Woodhead Publishing; 2017. p. 185-207.

[26] Al-Sharif M, Attom M. The Use of Burned Sludge as a New Soil Stabilizing Agent2000.
[27] Chen L, Lin D-F. Stabilization treatment of soft subgrade soil by sewage sludge ash and cement. Journal of Hazardous Materials. 2009;162(1):321-7.
[28] Lin D-F, Lin K-L, Hung M-J, Luo H-L. Sludge ash/hydrated lime on the geotechnical properties of soft soil. Journal of Hazardous Materials. 2007;145(1):58-64.
[29] Chen L, Lin D, Luo H. Utilization of Incinerated Sewage Sludge Ash/Cement for Soft Soil Improvement. 2019.
[30] Shi C. Studies on Several Factors Affecting Hydration and Properties of Lime-Pozzolan Cements. Journal of Materials in Civil Engineering. 2001;13(6):441-5.
[31] Rukzon S, Chindaprasirt P. Development of Classified Fly Ash as a Pozzolanic Material. Journal of Applied Science. 2008;8(6):1097-1102.
[32] Helmuth R. Fly ash in cement and concrete. Skokie, Ill: Portland Cement Assoc.; 1987.
[33] He GH, Sun JM, Wei XF, Wang CH, Chen Y, Chen JZ. Chemical behavior of clinotobermorite crystal in the process of fly ash comprehensive utilization. Journal of Synthetic Crystals. 2015;44(9):2379-2384.
[34] Acar I. CHARACTERIZATION AND UTILIZATION POTENTIAL OF CLASS F FLY ASHES: Middle East Technical University; 2013.
[35] Hwang K-Y, Seo J-Y, Phan HQH, Ahn J-Y, Hwang I. MgO-Based Binder for Treating Contaminated Sediments: Characteristics of Metal Stabilization and Mineral Carbonation. CLEAN – Soil, Air, Water. 2014;42(3):355-63.
[36] Bonaccorsi E, Merlino S, Biagioni C. The tobermorite supergroup: a new nomenclature. Mineralogical Magazine. 2015;79(2):485-95.
[37] Cuesta A, Zea-Garcia JD, Londono-Zuluaga D, De la Torre AG, Santacruz I, Vallcorba O, et al. Multiscale understanding of tricalcium silicate hydration reactions. Scientific Reports. 2018;8(1):8544.
[38] Lu J-X, Poon CS. Improvement of early-age properties for glass-cement mortar by adding nanosilica. Cement and Concrete Composites. 2018;89:18-30.
[39] Ng S, Guo J, Ma J, Loo SCJ. Synthesis of high surface area mesostructured calcium phosphate particles. Acta Biomaterialia. 2010;6(9):3772-81.